# UC Santa Barbara
## UC Santa Barbara Electronic Theses and Dissertations

**Title**

An improved climatological forecast method for projecting end-of-season Water Requirement Satisfaction Index (WRSI)

**Permalink**

https://escholarship.org/uc/item/8k95d4nz

**Author**

Turner, William Augustus

**Publication Date**

2020

Peer reviewed|Thesis/dissertation

UNIVERSITY OF CALIFORNIA

Santa Barbara


An improved climatological forecast method for projecting end-of-season Water

Requirement Satisfaction Index (WRSI)


A Thesis submitted in partial satisfaction of the requirements for the degree of Master of Arts

in Geography


By


William A Turner


Committee in charge:

Professor Charles Jones, Chair

Dr. Gregory Husak

Dr. Chris Funk

Professor Dar Roberts


September 2020

The thesis of William A Turner is approved.

_____
Charles Jones, Committee Chair

_____
Greg Husak

_____
Chris Funk

_____
Dar Robers

September 2020

An improved climatological forecast for projecting end-of-season Water Requirement

Satisfaction Index (WRSI)

ACKNOWLEDGEMENTS

In addition to my committee, I would like to provide thanks to the following:

to the Climate Hazards Center (CHC) for providing me with an incredible learning

environment, and financial support throughout my time at UCSB

to our editor, Juliet Way-Henthorne, for her unwavering patience

to Kate Voss and Laura Harrison for providing guidance as I traverse the circuitous path of

graduate school

to my friends and family for keeping me sane.

ABSTRACT

An improved climatological forecast for projecting end-of-season Water Requirement

Satisfaction Index (WRSI)

By

William A Turner

A simple—yet powerful—indicator used to monitor weather-related food insecurity is the

Water Requirement Satisfaction Index (WRSI). This water-balance model uses precipitation

(PPT) and potential evapotranspiration (PET) data to estimate the water supply and demand a

crop experiences over the course of a growing season. If the season is still in progress,

climatological forecast data can be adjoined with to-date conditions to provide insight into

potential end-of-season crop performance. However, if used incorrectly, these same

indicators can become a detriment to early warning, resulting in a lack of, or misallocation

of, precious humanitarian aid. While several prominent agencies and data centers use

arithmetic average climatological data as proxies for "average conditions," little published

research has evaluated the effectiveness of this forecast method when used in crop-water

balance models (i.e., WRSI). We use the WRSI hindcasts of three African regions' primary

growing seasons, from 1981-2019, to assess the adequacy of the arithmetic mean

climatological forecast. We find that this method of forecasting end-of-season (EOS) WRSI

results in crop-water condition predictions that are positively biased, i.e., they overestimate

WRSI. This bias ranges from 2-23% positive bias throughout portions of east, west, and

southern Africa. The proposed alternative is a scenario-based approach, which adjoins the

to-date conditions with data from previous seasons to produce a series of historically realistic

conclusions to the current season (one potential scenario generated from each year in the data

record; 1981-2019). The mean of these scenarios is then used as the projected end-of-season

WRSI, hereby referred to as the WRSI Outlook. We find this approach has a near-zero bias

score, and correspondingly, it has an improved (lower) Root Mean Squared Error (RMSE) in

comparison to the traditional arithmetic average climatological method. While an increase in

accuracy is a welcome by-product, the slight decrease (or increase, as seen during wet years)

in RMSE has less to do with forecast skill, and more to do with  the reduction of bias

provided by the mean-scenario method. In total, the findings from this paper highlight the

inadequacies of the existing arithmetic mean climatological forecast method when used to

project EOS WRSI and present a less-biased, and more accurate, mean scenario-based

approach.

TABLE OF CONTENTS

# 1   Introduction

As the five-year mark of the UN General Assembly 2030 Agenda for Sustainable

Development looms on the horizon, hunger is on the rise globally (FAO et al., 2019). A

recent Global Report on Food Crises by the World Food Programme (WFP) estimates that

135 million people across 55 countries are, or will be, in need of urgent humanitarian food

and nutrition assistance this year; of those, more than half are in Africa (WFP, 2020). Global

food security can be categorized as a disruption to one or more of the following pillars:

adequate food availability, food access, food utilization, stable prices, and incomes (Brown et

al., 2015). The destabilization of these pillars frequently stems from either conflict and

insecurity, or weather and climate (FAO et al., 2017). While conflict and insecurity has been

the predominant driver of food insecurity, weather extremes are increasingly significant

(WFP, 2020). Furthermore, when separated by key drivers, Africa had the largest numbers of

acutely food-insecure people in need of assistance in countries predominantly affected by

adverse weather events, particularly in east and southern Africa (FAO, 2019). Fortunately,

international aid agencies, national disaster risk management systems, and nongovernmental

organizations can often provide effective humanitarian relief by identifying and targeting the

most food-insecure populations for assistance (Funk et. al., 2019). In particular, the Famine

Early Warning System Network (FEWS NET)[1] assists by providing timely and localized

---

[1] FEWS NET partners and implementers include the U.S. Agency for International Development's Bureau for Humanitarian Assistance (USAID BHA), United States Geological Survey Earth Resource Observation and Science Center (USGS/EROS Center), National Aeronautics and Space Administration (NASA), National Oceanic and Atmospheric Administration (NOAA), Chemonics International, and the Climate Hazards Center (CHC).

agroclimatic information necessary for identifying those areas and populations most at risk of drought- or flood-induced food insecurity (Funk et. al., 2019). With early warning, appropriate interventions can be made (example: UNDP, 2018; DuBois et. al., 2018). However, if used incorrectly, these same indicators can become a detriment to early warning. Here, we document the tendency of one commonly used indicator for seasonal crop-water monitoring, the Extended Water Requirement Satisfaction Index (Extended WRSI), to systematically overestimate end-of-season (EOS) crop conditions when using arithmetic average climatology inputs (precipitation [PPT] and reference evapotranspiration [RefET]). In its place, we propose an alternative, mean scenario-based approach, which corrects for these biases and provides an improved means of projecting EOS crop conditions.

The timely and spatially focused monitoring products, seasonal outlooks, and agroclimatic alerts provided by FEWS NET and its partners guide humanitarian assistance, helping to save lives and secure livelihoods among some of the world's most food-insecure populations. Given the increasing attribution of climate and weather-induced food insecurity (SADC, 2016; Archer et. al., 2017; Funk et al., 2018, 2019; Shukla et al., 2020), there is an increased effort to expand upon and improve the ability to monitor agroclimatic conditions. Some existing methods use remote sensing and in situ data, including precipitation (Funk et al., 2015b) and evapotranspiration (Hobbins et al., 2020; Hobbins et al., 2019) products, and derived crop-water balance models. The WRSI, originally calculated with station rainfall and average dekadal reference evapotranspiration, has been shown to be directly related to crop yield data in Senegal, Algeria, Ethiopia, and Togo using linear yield-reduction functions (FAO, 1977; FAO, 1979; FAO, 1986; Lhomme et al., 1991). In addition to its use as a proxy

crop yield index, satellite rainfall-based WRSI simulations have been used to determine loss exceedance probability (LEP) curves for maize in Kenya, Malawi, and Mozambique, and for millet in Niger. Drought frequency maps indicating the drought return interval at the district level were used to indicate the agricultural drought risk characteristics for the selected crops (Jayanthi et al., 2014). However, to our knowledge, no research has been undertaken to investigate the implications of using arithmetic mean climatological inputs, neither in regards to the original formulation of using average evapotranspiration with time-specific precipitation, nor in the case of the Extended WRSI, which uses average PPT and RefET to project EOS WRSI.

The following three chapters are laid out as follows. Chapter 2, Materials and Methods, (1) first details the data used in the calculation of the WRSI in this thesis. (2) Next, we provide an in-depth documentation of the WRSI, describe the existing WRSI forecast methodology (Extended WRSI) and its shortcomings, and propose an alternative approach to a climatological forecast (the WRSI Outlook). Lastly, we detail the methods/metrics for testing the skill of both forecasts. Chapters 3 and 4 detail the bias and accuracy scores of each forecast method, and provide a discussion of the causes and implications of these results. Finally, Chapter 5 provides brief concluding remarks, including a summary of our findings, and a suggested way forward for WRSI forecasting.

# 2    Materials and Methods

## 2.1  Data

Climate Hazards InfraRed Precipitation with Stations

The Climate Hazards Group InfraRed Precipitation with Station data (CHIRPS) data set is a 30+ year, quasi-global rainfall data set, available at the monthly, dekad, pentad, and daily time steps. CHIRPS spatial coverage spans from 50°S-50°N (over all longitudes), with the data record extending from 1981 to near present. CHIRPS blends a high-resolution climatology (Funk et al. 2015a) with station data and inter-calibrated (Knapp et al. 2011) thermal infrared precipitation estimates to create a 0.05-degree native spatial resolution gridded rainfall time series appropriate for trend analysis and seasonal drought monitoring in data-sparse regions with complex terrain.

The CHIRPS product requires two steps for its operational production: (i) Pentadal rainfall estimates (five-day rainfall) are created from Cold Cloud Duration-based satellite data, which are obtained from regression models, and calibrated using TMPA 3B42. The pentadal estimates are converted to fractions of the long-term mean precipitation estimates, and are then multiplied by the Climate Hazards Center's Precipitation Climatology version 1 (CHPClim) (Funk et al. 2015a) data to remove the systematic bias. This outcome is named CHIRP. (ii) In situ observations from stations are blended with the CHIRP data using a

modified inverse distance weighting algorithm in order to produce CHIRPS (Funk et al., 2015b).

The creation of CHIRPS has supported drought monitoring efforts by the USAID Famine Early Warning Systems Network (FEWS NET), and has proven to be one of the most accurate rainfall products for characterizing wet seasonal cycles (Dunning et al., 2016; Salerno et al., 2019), climate variability (Dinku et al., 2007, 2018) and agricultural drought in Africa (Agutu et al., 2017; Ayehu et al., 2017; Ndayisaba et al., 2017; Zhan et al., 2016).

For use in the WRSI, CHIRPS is aggregated from daily to dekadal timesteps, and resampled to 0.1-degree resolution by the Climate Hazards Center. The climatology CHIRPS used in this study is calculated as the mean dekadal CHIRPS value from 1981 to 2019.

## Global Reference ET for the FEWS NET Science Community

The Global Reference Evapotranspiration for the FEWS NET Science Community (RefET) is produced by the National Oceanic and Atmospheric Administration's Physical Sciences Division (NOAA-PSD) (Hobbins et al., 2018, 2019a, 2019b, 2020). It is generated using atmospheric reanalysis data to calculate RefET using the American Society of Civil Engineers (ASCE's) Penman–Monteith formulation on a daily basis (Allen et al., 2005), which is used in many studies (e.g., McEnvoy et al., 2016a, b). RefET is driven by five MERRA-2 variables: 2-m air temperature (T2M), 2-m specific humidity (QV2M), surface downward shortwave radiation (SWGDN), 2-m wind speed at 2 m height (U2M and V2M), and surface atmospheric pressure (PS). The RefET is calculated for two different crop types: (i) long-crop, or a 0.5-m alfalfa reference crop; (ii) short-crop, or a 0.12-m short grass

reference crop. Daily RefET surfaces are spatially downscaled to 0.125° x 0.125° using climatological monthly potential evaporation (PET) estimates from the International Water Management Institute (IWMI). The manuscript detailing this data set is currently in progress. For more information, please visit the Global Reference ET for the FEWS NET Science Community [website](#).

For use in the WRSI, the short-crop RefET is aggregated from daily to dekadal timesteps, and resampled to 0.1-degree resolution by the Climate Hazards Center. The climatology RefET used in this study is calculated as the mean dekadal RefET value from 1981 to 2019.

## 2.2   Methodology

### 2.2A Water Requirement Satisfaction Index

Background

Our analysis revolves around the water requirement satisfaction index (WRSI). Frère and Popov originally proposed this simplified crop-weather analysis model in 1979 to the United Nations Food and Agriculture Organization (FAO) as a proxy for crop performance, and an indicator of the satisfaction of the crop water requirements in areas of the world where water represents the main constraint for crops (FAO, 1979; FAO, 1986). The components of this crop water balance model are depicted via a schematic diagram in Figure 1, and then described in detail in the text that follows.
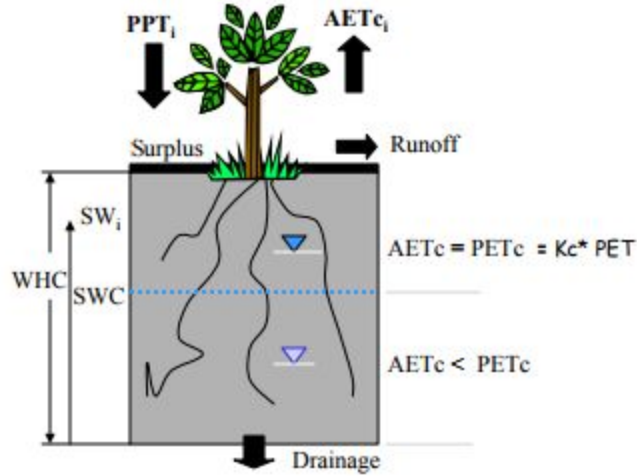
*Figure 1: A schematic diagram showing the components of a crop water balance model. Terms and variables involved will be described in more detail in the following text. Source: Characterization of yield reduction in Ethiopia using a GIS-based crop water balance model (Senay and Verdin, 2003).*

The WRSI is determined by the water supply and water demand a crop experiences during the growing season. The standard time step of analysis is the dekad, which splits the months into three parts; the first two dekads of a given month are 10 days long, and the third dekad completes the month (8-11 days) (WMO, 1992). Seasonal total water satisfaction is calculated by summing the corresponding dekadal values of the growing period. For a given monitoring interval (i.e., season) of *n* timesteps (i.e., dekads), WRSI is calculated as the ratio of actual crop evapotranspiration (AETc) to the crop water requirement, represented as the crop-specific potential evapotranspiration (PETc).

$$WRSI = \frac{\sum\limits_{i=1}^{n} AETc}{\sum\limits_{i=1}^{n} PETc} \times 100 \tag{1}$$

It is important to note here the relationship between ET, PET, RefET (also referred to in academic literature at $ET_0$), and AET. The distinction between these terms is described in

detail by the United Nation's Food and Agriculture Organization guidelines for calculating

crop evapotranspiration (FAO, 1998) and, more recently, in chapters seven and eight of

Twenty-First Century Drought Early Warning, Theory and Practice (DEWS) (Funk and

Shukla, 2020), but it can be summarized as follows. Evapotranspiration is traditionally

defined as the combined upward moisture fluxes of evaporation and transpiration. To put this

moisture flux in the context of atmospheric demand, the American geographer and

climatologist Charles Warren Thornthwaite (1899-1963) introduced the concept of "potential

evapotranspiration" (PET) as the amount of water which would evaporate and transpire from

a surface *if unconstrained by water supply* (Thornthwaite, 1948). While PET is the term most

frequently used in literature, the newer and more precise term is reference crop ET (RefET),

where *Ref* is referring to a 0.12-meter high, green-grass reference crop with defined

characteristics (FAO, 1998). The WRSI further adjusts the RefET using crop-specific

coefficients that vary based on the phenology of different cereals and grains.

$$PETc_i = Kc_i \times RefET_i \qquad (2)$$

The Kc values define the water use pattern of a crop based on the growth stage at that

point in the growing season. Published values (FAO, 1998) are available for critical points in

a crop phenology, and intervening values are linearly interpolated for each time step (dekad)

based on the length of the growing period (LGP) for that crop. The four crop growing phases

are emerging, vegetative, flowering (i.e., reproductive), and ripening (i.e., maturation). Our

analyses use millet as the crop type for west Africa, and maize for east and southern Africa.

For both crop types, the Kc value for the emerging stage, which spans from the start of

season (SOS) to the beginning of the vegetative phase, is 0.3. The timing of the succeeding

growth stages and corresponding Kc values for millet are as follows. The vegetative stage begins 14% into the LGP and ends at 38% of the LGP, with Kc values linearly interpolated from 0.3 to 1.0. The Kc during the flowering stage (38-76% of the LGP) is 1.0. The maturation stage spans the remainder of the season (76% to 100% of the LGP) with Kc values linearly interpolated from 1.0 to 0.3. Similarly, the timing of the growth stages and corresponding Kc values for maize are as follows. The vegetative stage begins 16% into the LGP and ends at 44% of the LGP, with Kc values linearly interpolated from 0.3 to 1.2. The Kc during the flowering stage (38-76% of the LGP) is 1.2. The maturation stage spans the remainder of the season (76% to 100% of the LGP) with Kc values linearly interpolated from 1.2 to 0.3. For context, Kc values greater than one indicate periods of the phenological cycle in which the crop has a greater upper limit to its atmospheric demand of moisture than the *reference* green-grass crop used in the calculation of the RefET data.

AETc, seen in the numerator of Equation 1, represents the actual (as opposed to the potential) amount of water withdrawn from the soil water reservoir, or Plant Available Water (PAW). Here, we must recognize that the hydrologic balance between upward (ET) and downward (i.e., PPT) fluxes at any given location and time will either be energy-limited or water-limited (Bouchet, 1963). In those locations and times where precipitation is in excess of evaporative demand, the balance will be energy limited, and thus, the actual amount of water vapor that evaporates and transpires from the soil and vegetation (actual ET or AET) will be capped by the RefET forcings (e.g., radiation, wind speeds, and vapor pressure deficit [VPD]) (Hobbins et al., 2012). In contrast, those times and places that are water limited will result in a water balance that is less than the net radiation balance, and thus, AET will be less

than RefET. This source-to-sink moisture imbalance results in a nuanced "complementary relationship" between RefET and AET, which was introduced by Bouchet (1963), and supported with observational evidence by Ramirez et al. (2005) and Hobbins et al. (2016). In general, neglecting heat storage, the energy balance at a given location on land is a function of the latent heat of vaporization, the amount of water vapor evaporated and transpired (AET), and the vertical advection of heat energy by atmospheric mixing in the planetary boundary layer (sensible heat flux). When there is ample soil moisture, evaporation occurs (water phase changes from liquid to vapor) and, correspondingly, latent heat increases. However, when a location is water limited and no new water inputs occur, latent heat will decrease due to the decrease in AET. More specifically, increased air temperature leads to an increase in saturation vapor pressure (SVP), while the lack of available moisture will lower the vapor pressure (VP). As such, the vapor pressure deficit will increase (*VPD = SVP - VP*). Given the VPD's place in the numerator of the equation for RefET, this increase in VPD results in an increase in RefET (Hobbins et al., 2016). In the context of the WRSI, which measures plant-water satisfaction as the ratio of AET:RefET, this relationship implies that when an area is experiencing water stress due to limited precipitation, AET will decrease due to lack of available soil moisture for evaporation, while RefET will increase due to increasing air temperature. As such, dry conditions, as measured by precipitation, can be exacerbated by increased atmospheric demand (RefET).

To identify whether a location is energy or water limited at a given time, and thereby account for the complementary relationship between potential and actual evapotranspiration, the WRSI model establishes an antecedent soil water balance (SW). Beginning six dekads

before a gridcell's start of season dekad (SOS), the SW is calculated via a simple difference equation

$$SW_i = SW_{i-1} + PPT_i - PETc_i \tag{3}$$

in which the PETc is calculated using a low crop coefficient, 0.15, appropriate for bare soil. The $SW_i$ is then carried to the next preseason dekad.

$$SW_{Preseason} = \sum_{i=SOS-6}^{SOS-1} SW_i \tag{4}$$

The value of SW (either a single dekadal instance, or the accumulated amount) ranges from a minimum of 0 (mm) to a maximum equal to the Water Holding Capacity (WHC) of the soil. If the $SW_i$ is negative, it is set to 0 before being passed to the next dekad; any $SW_i$ or $SW_{Preseason}$ greater than the WHC is assumed to be surplus (runoff or infiltration beyond the root zone), and, correspondingly, is set equal to the WHC. This baseline soil moisture is then passed into the first dekad of the growing season to initialize the Plant Available Water (PAW).

$$PAW = SW_{Preseason} + PPT \tag{5}$$

Before AET can be calculated, the Critical Soil Water (SWC) must be established. Where the soil is sufficiently wet, the soil supplies water fast enough to meet the atmospheric demand of the crop, and water uptake equals PETc. But, as the soil water content decreases, water becomes more strongly bound to the soil matrix and is more difficult to extract. When the soil water content drops below a threshold value, the SWC, soil water can no longer be

transported quickly enough towards the roots to respond to the transpiration demand, and the

crop begins to experience stress (AETc will be less than PETc). The SWC is a function of

local parameters for effective rooting depth fraction (RDF), water holding capacity (WHC),

and soil water fraction (SWF).

$$SWC_i \ = \ RDf_i \times WHC \times SWf \qquad \qquad (6)$$

RDF ranges from 0 to 1 during the growing season. It increases linearly from emergence

until the middle of the growing season when it attains effective depth (RDF = 1). The use of

the root depth fraction is meant to simulate where in the soil profile a crop's roots are

concentrated, given its growth stage (Senay and Verdin, 2003). The relevant soil information

(e.g., WHC and SWF) is from the FAO-UNESCO soil map of the world (1988), and

topographical parameters are derived from the GTOPO30 digital elevation model (DEM)

(Gesch et al., 1999). SWF is the fraction of WHC that defines transpiration stress (FAO,

1998). This can be thought of as a resistance term, with higher resistance to water extraction

resulting in increased susceptibility to water stress. For context, the SWF for millet and

maize is 0.4 and 0.45, respectively, indicating that maize is less drought tolerant than millet.

For additional details, see Senay and Verdin (2003), Verdin and Klaver (2002), and Crop

Evapotranspiration: Guidelines for Computing Crop Water Requirements (FAO, 1998).

With the antecedent soil moisture set, the AET can be calculated. The following

procedure was pieced together from personal communication with Tamuka Magadzire—one

of the developers of the GeoWRSI software, and a regional scientist with the Climate

Hazards Center. However, to our knowledge, this is the first known formal documentation of

the two-step estimation of AET used in the WRSI. The total crop evaporative demand

(AETc) is calculated in two steps, or "burns." The first burn, AET1, is the amount of evapotranspiration from the initial soil-water balance (PAW1). This is presumed to be the most readily available soil moisture, and therefore, has a high extraction coefficient (Crop$_{C1}$; standard value of 0.75). The second burn, AET2, is the amount of soil water the plant extracts if/when there is soil moisture remaining after the first burn (PAW2). As this is a smaller, less accessible amount of available water to pull from, the coefficient is lower (Crop$_{C2}$; standard value of 0.25). We show this process using a decision tree diagram in Figure 2.
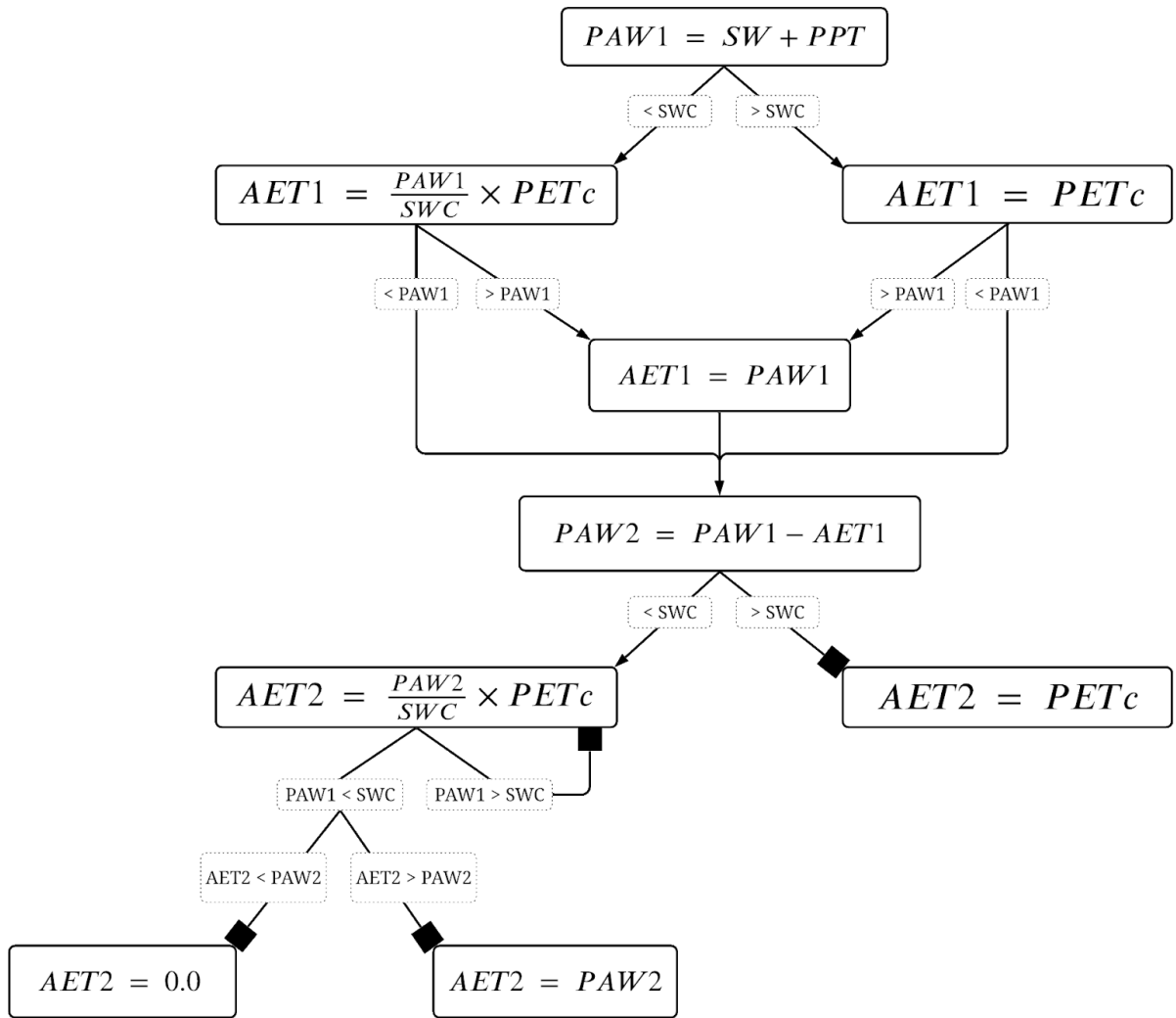
*Figure 2: A decision tree diagram showing the two-burn calculation of actual evapotranspiration (AET) for a given time interval (i.e., dekad). Flow direction is top to bottom (PAW1 to AET2). Equations are enclosed in solid-bordered boxes. Connecting lines (branches) with arrows are decision nodes, with dotted boxes containing the conditional statement associated with the previous equation. End nodes are indicated with solid, filled black squares. The variables involved are described in more detail in the preceding text.*

Each burn (AET1 and AET2) is multiplied by its corresponding extraction coefficient

($Crop_{C1}$ and $Crop_{C2}$, respectively), and summed to attain the total AETc for that dekad.

$$AETc_i = (Crop_{C1} \times AET1) + (Crop_{C2} \times AET2) \tag{7}$$

14

AETc and PETc are calculated for each dekad of the growing season, beginning at the onset of rains (SOS). The end of season (EOS) WRSI is reported as the seasonal total crop-water demand divided by the seasonal total potential evaporative demand:

$$WRSI = \frac{\sum\limits_{i=SOS}^{EOS} AETc_i}{\sum\limits_{i=SOS}^{EOS} PETc_i} \times 100 \qquad (8)$$

The SOS is determined using a threshold amount and distribution of rainfall received in three consecutive dekads, as defined by the Centre Regional de Formation et d'Application en Agrométéorologie et Hydrologie Opérationnelle (AGRHYMET, 1996). SOS is established when there is at least 25 mm of rainfall in an initial dekad, followed by a total of at least 20 mm of precipitation in the following two consecutive dekads. Once these rainfall metrics are met, the SOS is defined as the first dekad in that 3-dekad series. The EOS is then defined by adding the gridcell LGP to the SOS dekad and subtracting one.

The WRSI, originally calculated with station rainfall and average dekadal reference evapotranspiration, was shown to be directly related to crop yield data in Senegal, Algeria, Ethiopia, and Togo using linear yield-reduction functions (FAO, 1977; FAO, 1979; Lhomme et al., 1991). In theory, a situation of "no deficit" (i.e., EOS WRSI = 100) corresponds to normal crop yields, while a value less than 100 is associated with reduced crop yields. In actuality, the range of WRSI values and correlation to above/below-average yields varies depending on the region. As such, the most common form of the WRSI used as a monitoring tool is the percent of average (POA), which normalizes the end-of-season WRSI by dividing by the historical median end-of-season WRSI. Quasi-global gridded data sets, such as

CHIRPS and the reference evapotranspiration data set used in this thesis, allowed this

process to be adapted and extended from a single station location to a gridcell-based

geospatial application (GeoWRSI) (Verdin and Klaver, 2002), in which each gridcell is

treated like a station from the classic FAO (1977) method. Although there are many more

robust and data-intensive, physically based crop models available, FEWS NET adapted the

FAO WRSI model for implementation in 2002 because of its limited data requirements,

simplicity in operational use, and ability to capture spatially varying crop-water satisfaction

in data-sparse areas around the world (Senay and Verdin, 2003). Most recently, the Climate

Hazards Center implemented the GeoWRSI model in Interactive Data Language (IDL) to

facilitate simulations using varying precipitation and evapotranspiration inputs, including

forecast data for use in current season monitoring. To ensure consistency, this IDL

implementation of the WRSI model is used for all WRSI runs and comparisons in this study.

## USGS/EROS Extended WRSI

The Extended WRSI is provided by the USGS FEWS NET Project, which is part of

the Early Warning Focus Area at the USGS Earth Resources Observation and Science

(EROS). The Extended WRSI is a forecast estimate of what the WRSI would be at the end of

the growing season, assuming the dekadal precipitation and evapotranspiration for the

remainder of the season matches the historical average (also known as an arithmetic mean

climatological forecast). At a given point in a monitored growing season, long-term average

climatological data are used to fill in the missing data between the current dekad and the end

of the season. Once that is done, the calculation principles are the same as the standard WRSI

16

(ratio of the season total crop evapotranspiration to the crop water requirement). As the season progresses, and actual PPT and RefET data become available, the climatology data previously used for those dekads are replaced so that at the end of the growing season, only current-year PPT and RefET are used as inputs. It is important to note here that this methodology is not meant to be a forecast that is responsive to existing/prevailing climate conditions, but rather, a baseline estimate of what the EOS WRSI would be if the remainder of the season resembled the average of years past. The problem arises when the methodology systematically misrepresents "average" conditions.

The motivation for this thesis stems from an observed tendency of this Extended WRSI method to be overly optimistic (i.e., produce above-average projected anomalies), particularly early in the monitoring season. The source of this erroneous reporting is due to two significant shortcomings. First, several studies have shown that precipitation and evapotranspiration covary. More specifically, there tends to be a non-linear inverse relationship; evapotranspiration tends to be lower (higher) during rainy (dry) days, primarily as a result of decreased (increased) solar radiation and increased (decreased) relative humidity (Bruno Collischonn and Walter Collischonn, 2016). Furthermore, as described in the previous section, there exists a complementary relationship between actual evapotranspiration and reference evapotranspiration, which can exacerbate dry conditions. This is especially important and apparent when monitoring drought years, as below-average rainfall conditions are exacerbated by above-average evapotranspiration, resulting in two-fold water stresses. Long-term averages of precipitation and evapotranspiration fail to capture these finer time scale interplays between PPT, AET, and RefET, and as such, the

17

historical WRSI calculated with average dekadal evapotranspiration has considerably lower variability than does WRSI calculated with time-specific data (Figure 3). The second, and perhaps more profound shortcoming of using climatology inputs to predict EOS WRSI, is that using average precipitation results in heavily biased EOS WRSI projections, especially when used early in the season. This is primarily due to consistently wet days (> 0 mm), which are inherent in any historical average calculation. On the other side of the coin, marginal cropping zones with short rainy seasons rely on above-average rainfall events to recharge soil moisture and satisfy crop-water demands, and thus, "average" inputs result in consistently below-average projected WRSI (dry bias). Regardless of the directionality of the bias, any reduction in variability resulting from a failure to use time-specific data (as opposed to averaged data) limits our ability to place current events in context with historical precedents—a practice that is integral to index-based insurance and consequent resource allocation (food and humanitarian assistance). This study aims to reduce the biases associated with using climatology inputs by introducing more historically relevant hydroclimatic data, thereby improving EOS projections, and subsequent monitoring efforts to timely and adequately allocate food and humanitarian assistance.
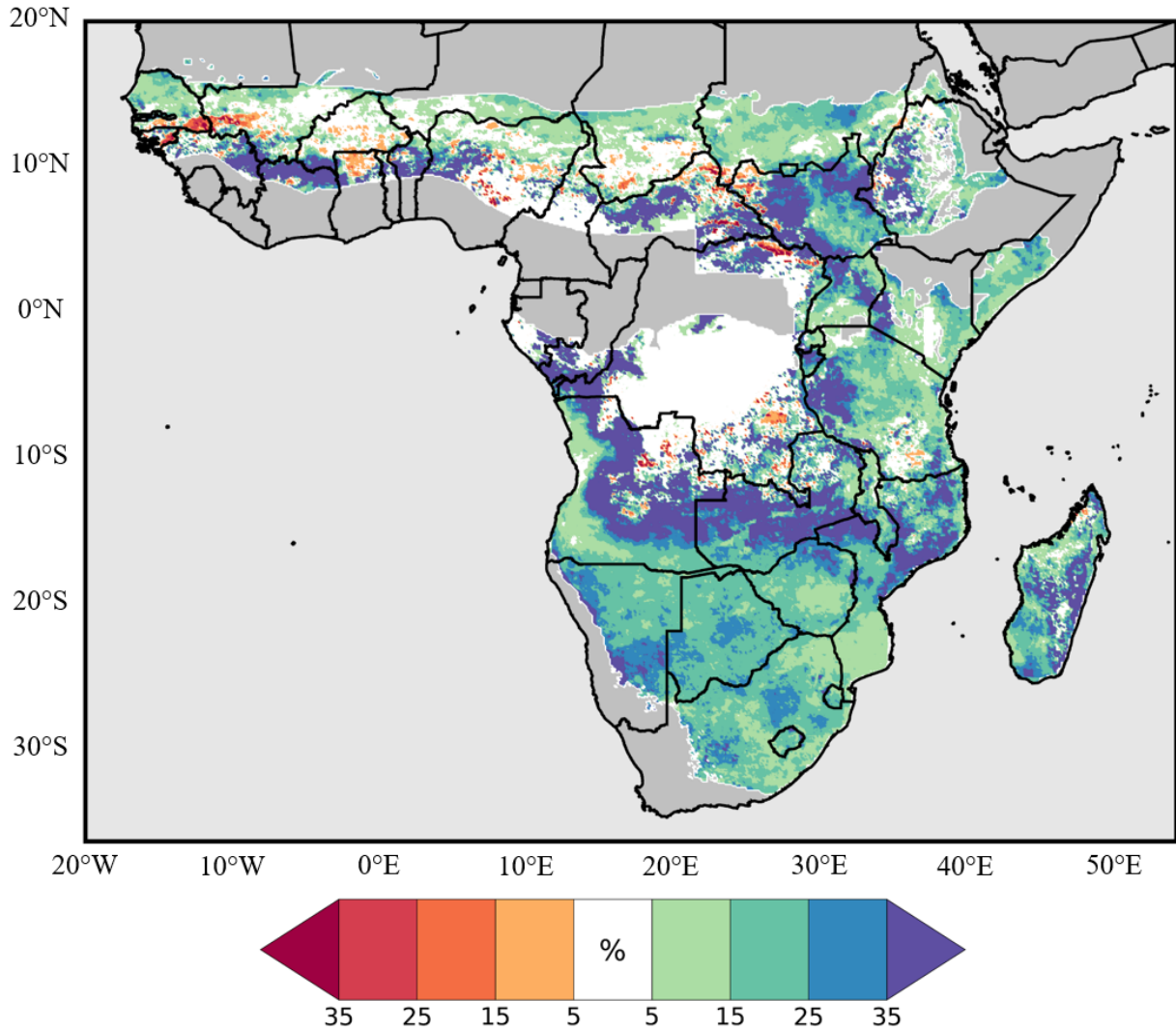
*Figure 3: Change in the standard deviation of historical (1981-2019) end-of-season WRSI when using time-specific evapotranspiration, instead of average (climatology) values, in west, east, and southern Africa growing seasons. Blue (red) hues indicate areas where the variability of EOS WRSI increases (decreases) with the addition of time-specific RefET in place of climatology RefET.*

## WRSI Outlook

The proposed alternative, the WRSI Outlook, is a mean scenario-based approach, which uses all available precipitation and evapotranspiration seasons from 1981-2019 to produce historically relevant end-of-season WRSI scenarios. Whereas the Extended WRSI

method uses average PPT and RefET to fill in the gap from the current dekad and the end of the season, the WRSI Outlook fills in the missing series of dekads with historical (e.g., 1981, 1982, 1983) PPT and RefET data for the same period, with each set of year-specific data resulting in one potential EOS scenario; what would the EOS WRSI be if the remainder of the forecasted year looked exactly like that period in 1981? 1982? 1983? And so on. The average (mean) of these potential scenarios is calculated to produce the WRSI Outlook. Figure 4 shows this process at the gridcell level, and can be described in more detail as follows. For a given monitoring season, the first opportunity for a WRSI Outlook is the first dekad after an SOS is identified (the start of the fourth dekad of a gridcell's growing period). Each potential scenario uses these first three dekads of to-date PPT and RefET, adjoined with PPT and RefET data from each year in the historical record (1981-2019). Assuming the monitoring year is 2020, and the SOS for a given gridcell is dekad 10 (April 1st, 2020), PPT and RefET data are coupled with 1981 data from dekad 13 (May 1st) to dekad 33 (November 30th). This composite scenario is used to calculate one potential EOS WRSI for the 2020 monitoring season for that gridcell. The same process is performed for each of the remaining years in the historical record, for each gridcell in the region that has recorded an SOS in 2020. For the west and east (southern) Africa growing season, this equates to a maximum of 39 (38) potential scenarios per gridcell. In testing, we found that historical scenarios that did not actually record enough PPT to meet the SOS metrics (25 mm in one dekad, followed by two consecutive dekads summing to 20 mm) in their own year resulted in a significant underestimation of the projected EOS WRSI (dry bias). As such, these no-start scenarios are removed from the mean-scenario calculation; e.g., when projecting the 2020 season for a

20

specific gridcell, if that gridcell did not actually record an SOS in 1981, then 1981 data would not be used in the collection of potential 2020 scenarios. The arithmetic mean of the remaining potential scenarios is used as the WRSI Outlook.
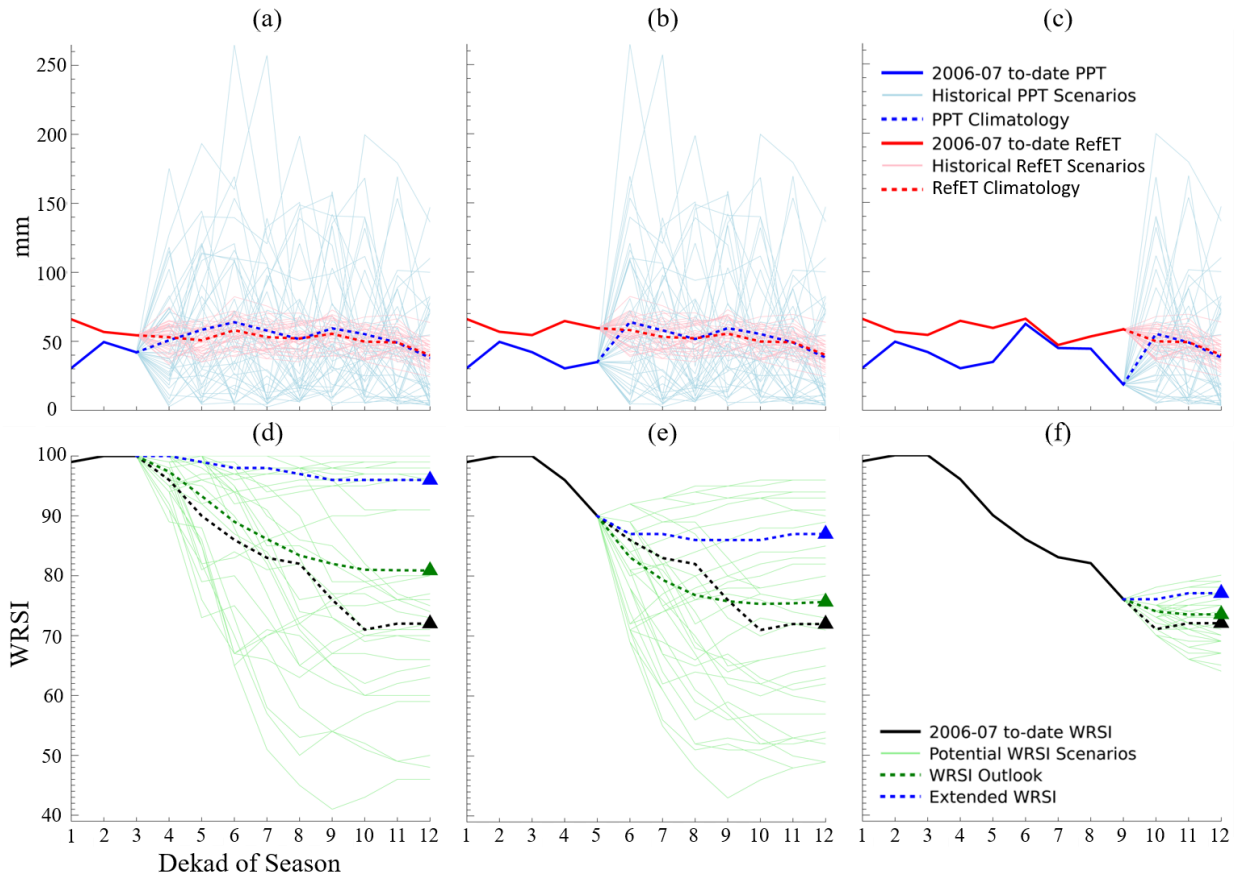


*Figure 4: The scenario WRSI process for a single gridcell in southern Africa (Zimbabwe), shown for three separate hindcast opportunities of the 2006-07 growing season in southern Africa (Zimbabwe). This particular gridcell has an LGP of 12 dekads. The top row of plots (4a, 4b, and 4c) show how to-date (2006) PPT (solid, thick blue line) and RefET (solid, thick red line) is adjoined with historical data (1981-2019, sans 2006) to create a series of scenarios. The adjoined historical PPT is indicated by thin, light blue lines; adjoined historical RefET is indicated by thin, light red lines. The dotted blue and red lines represent the long-term PPT and RefET climatologies (1981-2019 dekadal averages), respectively. The bottom row of plots (4d, 4e, and 4f) show each of the associated potential WRSI scenarios, calculated using the PPT and RefET scenarios from 4a, 4b, and 4c. The thin green lines are potential WRSI scenarios calculated using the adjoined historical PPT and RefET scenarios*

21

*(light blue and red lines from 4a, 4b, and 4c). The dotted green line indicates the mean of these historical scenarios, with the solid green triangle indicating the end-of-season WRSI Outlook. The dotted blue line indicates the calculated WRSI using climatology inputs (the dotted blue and red lines from the 4a, 4b, and 4c), with the solid blue triangle indicating the end-of-season Extended WRSI. The dotted black line indicates the actual WRSI for the 2006-07 season, with the solid black triangle indicating the true end-of-season WRSI for this gridcell season.*

This process is performed for each gridcell, at each hindcast opportunity of the growing period, for every year (1981-2019) to compare the bias and accuracy of both the Extended WRSI and WRSI Outlook; the hindcast error testing procedure will be described in more detail in the following section. In Chapter 3, we show the results of this testing, but a few observations can be made from Figure 4. (1) The observed covariability between PPT and RefET is lost when simply using long-term averages (climatologies). (2) Average dekadal PPT, when calculated for a known wet season, results in dekadal precipitation values that are consistently well-above zero, a phenomena which is unlike the natural intraseasonal variability of precipitation (well-above average dekads interspersed with near-zero dekads). In contrast, the WRSI Outlook uses historical, coupled precipitation and evapotranspiration data to create scenarios which are inherently more realistic potential conditions for the remainder of the season. This results in an estimate much closer to the initial intention of the Extended WRSI: *what would the EOS WRSI of the forecasted season be if the remainder of the season resembled the average of years past?*

## 2.2B Hindcast Error Testing

To compare the two WRSI forecast methods, we performed hindcasts, using both methods, at every time step in the historical record (1981-2019). For west and east Africa,

whose growing seasons are contained within the calendar year (April to November for west Africa, and February to November for east Africa), the maximum number of hindcast seasons is 39; the southern Africa growing season (September to May) crosses the calendar year, and as such, the maximum is 38 (1981/82 – 2018/19). There can be no hindcast for a season that does not have an SOS, and so, a given gridcell may have fewer hindcast seasons depending on its no-start frequency. Within a single hindcast season, a given gridcell, with, say, a length of growing period (LGP) of 12 dekads, has eight forecasting opportunities per season; one at the point the SOS has been identified (dekad four of the season), and once per dekad of the season up until one dekad before the end of the season (i.e., dekad 11). At each point, the performance of the hindcast was measured by comparing each method's projected WRSI to the actual EOS WRSI for that historical season. The two forecast performance metrics used in this study are Multiplicative Bias (hereby, simply referred to as *bias*) and Root Mean Square Error (RMSE). The bias of the forecast method for a given gridcell is calculated as:

$$Bias = \frac{\frac{1}{N}\sum_{i=1}^{N} F_i}{\frac{1}{N}\sum_{i=1}^{N} O_i} \times 100 - 100 \tag{9}$$

where N is the total number of predicted WRSI seasons (described above), F is the predicted EOS WRSI (either the Extended WRSI or the WRSI Outlook), and O is the observed (true) EOS WRSI for that season. Traditionally, the potential bias values range from -∞ to +∞, with a score of 1, implying the forecast method as no multiplicative bias. The formula shown here multiplies the traditional bias formula by 100 to convert the bias to a percentage of the mean historical WRSI, and then subtracts by 100 for ease of dry/wet bias interpretation. As such,

the multiplicative bias values shown here range from -∞ to +∞, with a value of 0% indicating the forecast method has no bias.

The accuracy of the forecast method for a given gridcell is calculated using the RMSE as follows:

$$RMSE = \sqrt{\frac{1}{N} \sum_{i=1}^{N} (F_i - O_i)^2} \qquad (10)$$

Simply put, the RMSE measures "average" error, weighted according to the square of the error. The RMSE does not indicate the direction of the deviations, but does put greater influence on larger errors than smaller errors. The range of values are from 0 to 100, with 0 constituting a perfect score (i.e., the forecast method's average prediction is equal to the true event).

The results discussed below focus on the forecast bias and accuracy at the first forecast opportunity (dekad four of the season), as this is when the disparity between the two methods is most apparent. As the season progresses, there is less remaining season to forecast, and so the two methods' projections converge on the actual EOS result. The RMSE is reported for all hindcast years (as described above), as well as for three subsets of the hindcast years. The subsets are divided based on the true end-of-season percent-of-average WRSI for each of the historical years, with cutoffs at below 90% of average, and above 110% of average. These designations are based on the standard color bars used in percent-of-average WRSI graphics popular for in-season monitoring (i.e., the USGS/USAID WRSI Anomaly map); <90% is the first color indicating below-average conditions, and conversely, >110% is the first color cutoff indicating above-average conditions. The purpose

of these subsets is to identify if one of the forecast methods performs better or worse during dry, average, or wet years. For a given gridcell, the *dry season* RMSE is calculated using only the hindcasts of seasons in which the true outcome was less than 90% of the historical average WRSI. The *average season* RMSE is calculated using only the hindcasts of seasons in which the true outcome was between 90% and 110% of the historical average WRSI. And, finally, the *wet season* RMSE is calculated using only the hindcasts of seasons in which the true outcome was greater than 110% of the historical average WRSI. For example, the *dry season* RMSE indicates the expected forecast error when forecasting an event with a known outcome of less than 90% of average. As the WRSI variability ranges considerably spatially, the number (N) of *dry/average/wet seasons* will vary for each gridcell.

## 2.3   Regions of Interest
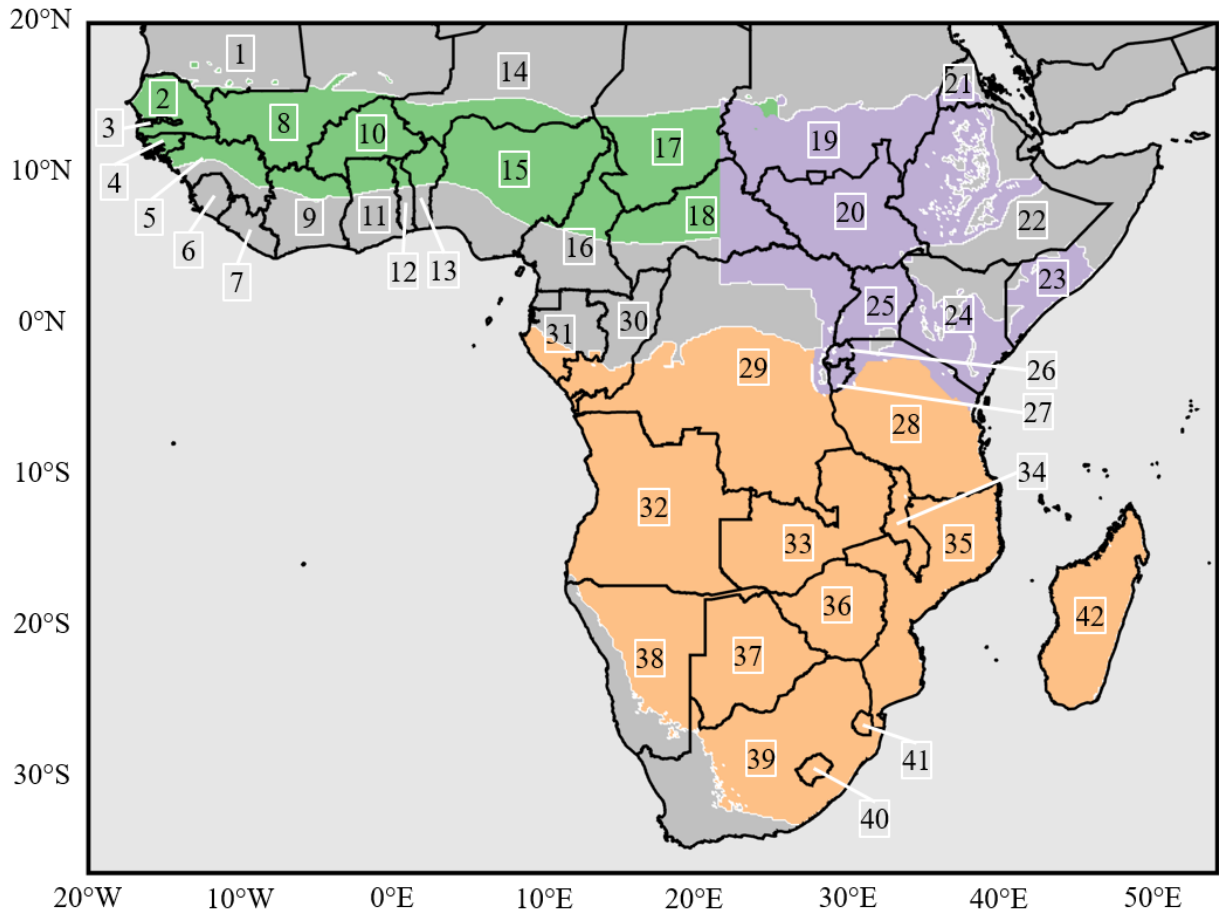


Figure 5: The three regions of interest are west Africa (green), east Africa (purple), and southern Africa (orange). The countries which reside in these WRSI-defined growing areas are labeled numerically, and listed as follows: **west Africa**: (1) Mauritania, (2) Senegal, (3) The Gambia, (4) Guinea-Bissau, (5) Guinea, (6) Sierra Leone, (7) Liberia, (8) Mali, (9) Côte d'Ivoire, (10) Burkina Faso, (11) Ghana, (12) Togo, (13) Benin, (14) Niger, (15) Nigeria, (16) Cameroon, (17) Chad, and (18) Central African Republic; **east Africa**: (19) Sudan, (20) South Sudan, (21) Eritrea, (22) Ethiopia, (23) Somalia, (24) Kenya, (25) Uganda, (26) Rwanda, and (27) Burundi; **southern Africa**: (28) Tanzania, (29) Democratic Republic of the Congo, (30) Republic of the Congo, (31) Gabon, (32) Angola, (33) Zambia, (34) Malawi, (35) Mozambique, (36) Zimbabwe, (37) Botswana, (38) Namibia, (39) South Africa, (40) Lesotho, (41) Eswatini, and (42) Madagascar.

This study focuses on the primary growing season for three sub-Saharan regions of interest in west Africa (WA), east Africa (EA), and southern Africa (SA). Approximately 52% of the global number of individuals predicted to be acutely food insecure in 2020 reside in these three regions (WFP, 2020; FAO 2019). Weather extremes are anticipated to be the predominant driver of 13%, 48%, and 37% of those affected in WA, EA, and SA, respectively (WFP, 2020).

The monitoring period for WA begins on the 10th dekad of the year (April 1st) and concludes on the 33rd dekad of the year (November 30th). While east Africa has a bimodal rainfall pattern, and correspondingly has two distinct growing seasons, this study focuses on the primary, or *long rains*, growing season. The monitoring period for the *long rains* growing season begins on the 4th dekad of the year (February 1st) and concludes on the 33rd dekad of the year (November 30th). In southern Africa, the monitoring period begins on the 25th dekad of the year (September 1st) and concludes on the 15th dekad of the following calendar year (May 31st).

These monitoring windows are designed to confine the time frame during which an SOS can occur to best correspond with likely planting dates. Once the SOS for a given season has been identified, the WRSI is only calculated based on the PPT and RefET during the designated LGP for that gridcell. All three regions have default land masks, produced by the FAO, incorporated in the GeoWRSI to focus monitoring on rainfed agricultural zones. We further refined the regions of interest by masking out areas that failed to start more than 33% of the historical record (one-in-three event, since 1981). The reasoning for this is that these areas are more likely to either (1) not be cropped areas or (2) practice rangeland

subsistence farming, which uses adaptive cropping strategies that differ from the standard parameters built into the WRSI model (greater crop row spacing, irrigation, etc.)(FAO, 1998). As such, the standard WRSI model is not ideal for monitoring cropping conditions in those areas.

# 3    Results

The results presented here first address the significant biases associated with the standard climatology method (i.e., USGS Extended WRSI), relative to the proposed mean scenario method (i.e., WRSI Outlook). Next, we investigate the accuracy of the two methods, as measured by the RMSE for all hindcasts, as well as for dry, average, and wet seasonal subsets. For both metrics, the results below are for the first forecast opportunity (dekad four of the season), as this is when the disparity between the two methods is most apparent. As the season progresses, forecast data is replaced with prevailing conditions for the season in question, there is less remaining season to forecast, and so the two methods' projections converge on the actual EOS result. Our results find that the CHC Outlook WRSI mean scenario method considerably reduces the magnitude of the biases of the Extended WRSI climatology method in areas of all three regions (e.g., west, east, and southern Africa). Correspondingly, the conservative (unbiased) nature of the CHC Outlook WRSI lends itself to having higher (or equivalent) overall accuracy in all three regions. In particular, the absence of a wet bias in the WRSI Outlook results in markedly reduced error in projecting below-average WRSI. Overall, the results of the CHC Outlook using mean scenarios are

highly encouraging, and are a marked improvement to the existing method of using

climatology inputs (i.e., Extended WRSI), particularly in regards to the reduction in bias.
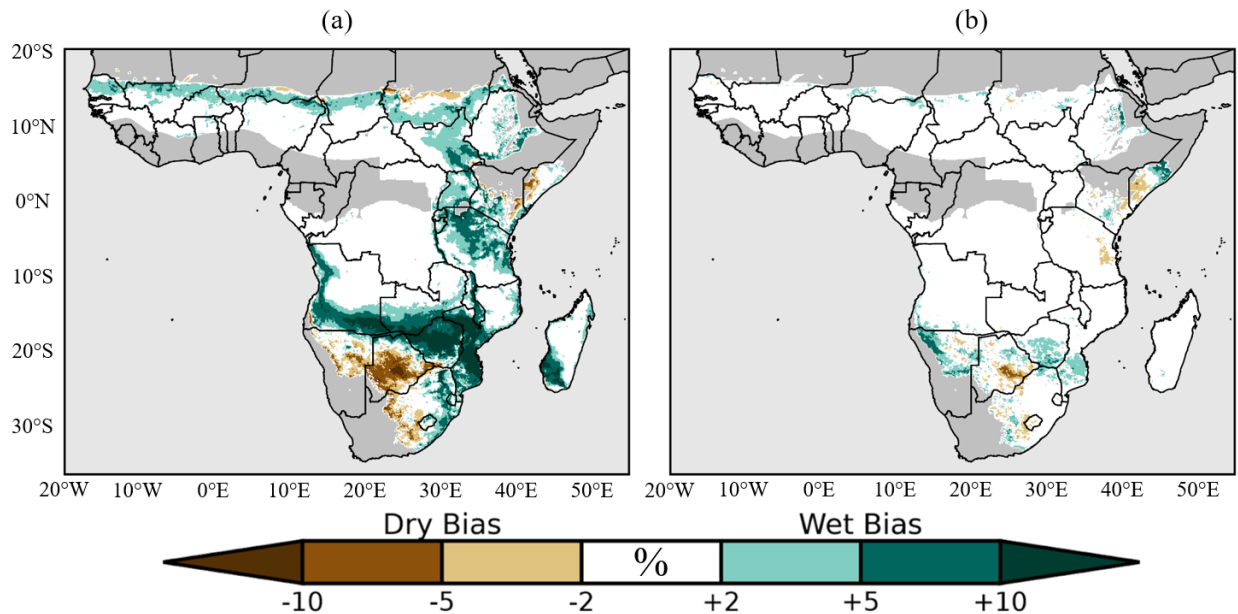
## 3.1 Bias



*Figure 6: Multiplicative bias, represented as the percent deviation from the mean historical WRSI, of the two end-of-season (EOS) WRSI forecast methods, taken at the first opportunity of a forecast (i.e., dekad four of the season) for west, east, and southern Africa growing seasons (1981-2019). Brown (blue) hues indicate areas where the forecast method has a dry (wet) bias, meaning the average forecast is less than (greater than) the true event outcome. White indicates areas where the forecast method is relatively unbiased (i.e., the average forecast is within +/- 2% of the true outcome). (a) Multiplicative bias of the Extended WRSI method, which uses climatology (average) inputs to predict end-of-season WRSI. (b) Multiplicative bias of the WRSI Outlook, which predicts the end-of-season WRSI by calculating the mean of a series of scenarios based on year-specific historical data.*

The primary initiative for this study is to detail the presumed bias associated with the

Extended WRSI, which uses climatology (average) precipitation and evapotranspiration

inputs. Systematic biases in EOS projections, whether they are underestimating or

overestimating, can have serious implications in regards to monitoring and subsequent

humanitarian aid efforts. Overly optimistic outlooks may result in certain areas

systematically being excluded from more fine-detail monitoring reports, thereby inhibiting

timely responses. Systematic underestimations (pessimistic outlooks) can also result in

attention being directed to  the wrong areas. In either case, precious attention and resources

are being allocated in the wrong locations, and thus, inhibiting timely and necessary aid.

In taking the average Extended WRSI at the first opportunity of a forecast (dekad 4)

in the forecast season and comparing it to the actual average historical EOS WRSI, we find

that the climatology method has a substantial *wet bias* (average forecasted WRSI is greater

than the average true WRSI) in all three regions (Figure 6a). In west Africa, the average

extended WRSI has a 2-10% wet bias throughout the northern half of the region (e.g.,

Senegal, southern Mali, northern Burkina Faso, southern Niger, northern Nigeria, and

southern Chad). In east Africa, the average Extended WRSI has at least a 2-5% wet bias

throughout much of the region, and has a 5-10% wet bias in eastern Sudan, southeastern

South Sudan, central Ethiopia, eastern Uganda, southwestern Kenya, Rwanda, and northern

Tanzania. The Extended WRSI also has a 2-10% dry bias in central Sudan, southern Somalia,

and central Kenya. The biases associated with the Extended WRSI are most severe in

southern Africa, where the wet bias is greater than 5% throughout the central and eastern half

of the region, and ranges from 10-23% in southeastern Angola, southern Zambia, Zimbabwe,

Mozambique, eastern Malawi, eastern South Africa, and southern Madagascar. Additionally,

the Extended WRSI has a considerable dry bias (2-10%) in northern Namibia and central

South Africa, and exceeds 15% in central Botswana. In contrast, the WRSI Outlook has a

near-zero bias throughout the three regions, with biases only exceeding +/- 5% in parts of

northcentral Ethiopia, southern Somalia, northern Namibia, southern Botswana, and southern

Zimbabwe (Figure 6b). With the exception of the five locations just listed, the magnitude of

the WRSI Outlook bias is smaller than that of the Extended WRSI bias in all areas. There are

no areas in which the WRSI Outlook bias exceeds 10%.
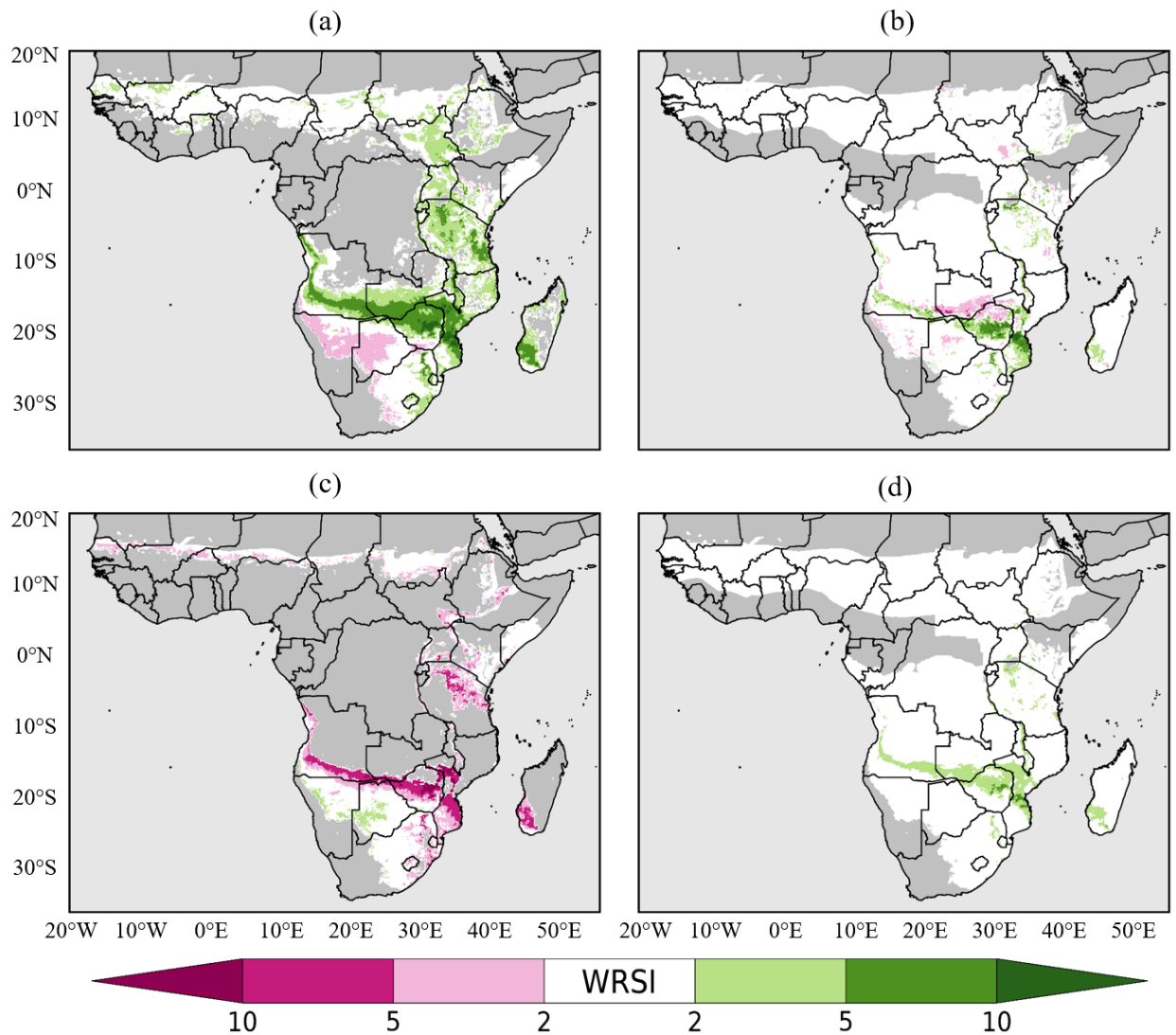
## 3.2   Accuracy



*Figure 7: Difference of average Root Mean Squared Error (RMSE) between the two end-of-season (EOS) WRSI forecast methods, taken at the first opportunity of a forecast (i.e., dekad four of the season) for west, east, and southern Africa growing seasons (1981-2019). Pink (green) hues indicate areas where the Extended WRSI using climatology inputs has a*

*smaller (greater) RMSE than does the WRSI Outlook using the mean scenario method. White indicates areas where the average RMSE of the two forecast methods is within 2 WRSI units of each other (i.e., the two methods have equivalent accuracy). The four panels show the average difference in RMSE between the two methods for: (a) years in which the true EOS WRSI is <90% of average (dry years); (b) years in which the true EOS WRSI is 90-110% of average (average years); (c) years in which the true EOS WRSI is >110% of average (wet years); (d) all years.*

While assessing the bias of the two forecast methods is the primary focus, there is an implicit interest in the accuracies of the two. The desired expectation is that the results will provide sufficient empirical evidence of (1) the shortcomings and inaccuracies of the existing Extended WRSI and (2) the improved methodology provided by the WRSI Outlook for unbiased and accurate prediction of end-of-season crop water requirements.

Figure 7 shows the difference in RMSE between the two methods in dry (Figure 7a), average (Figure 7b), wet (Figure 7c), and all (Figure 7d) seasons. The results correspond well with the expectations outlined previously. In areas where the biases of the two products are nearly equal, their RMSE values are also near equal. **Dry Seasons (Figure 7a)**: In areas where the Extended WRSI has a considerable wet bias, the WRSI Outlook has a smaller RMSE. In east Africa, the WRSI Outlook has an RMSE that is 2-10 WRSI less than that of the Extended WRSI in south Sudan, central Ethiopia, Uganda, southern Kenya, and northern Tanzania. In southern Africa, the WRSI Outlook has an RMSE that is 2-10 WRSI less than that of the Extended WRSI in Tanzania, Malia, southern Angola, Zambia, South Africa, and Madagascar, and 10-15 WRSI units less than the Extended WRSI RMSE in central Zimbabwe and central and southern Mozambique. In northern Namibia, Botswana, and western South Africa, where the Extended WRSI has a considerable dry bias, the CHC WRSI RMSE is 2-5 WRSI units larger than the Extended WRSI's RMSE. **Average Seasons**

**(Figure 7b)**: The RMSE of the two methods are fairly comparable in west and east Africa. In southern Africa, where the Extended WRSI bias exceeds 10%, the RMSE of the WRSI Outlook is 2-14 WRSI units smaller than that of the Extended WRSI in southern Angola, central Zimbabwe, and southern Mozambique. In southern Zambia and northern Zimbabwe, where the Extended WRSI has a 5-10% wet bias and the WRSI Outlook bias is near-zero, the Extended WRSI RMSE is 2-7 WRSI units less than that of the WRSI Outlook. This implies that the natural distribution of the historical (true) WRSI has a long tail of low values which pulls down the mean WRSI more than the median WRSI (left skew), which would lend itself to a method with a wet bias having a lower RMSE than one with no bias. **Wet Seasons (Figure 7c)**: As previously stated, the systematic wet bias of the Extended WRSI lends itself to having a lower RMSE during above-average (wet) seasons. In west Africa, the RMSE of the Extended WRSI is 2-5 WRSI units lower than that of the WRSI Outlook in the northern most parts of the region, including northern Senegal, central Mali, northern Burkina Faso, southern Niger, and central Chad. In east Africa, the RMSE of the Extended WRSI is 2-10 WRSI units lower than that of the WRSI Outlook in southern Sudan, southeastern South Sudan, central Ethiopia, southern Uganda, southwestern Ethiopia, and northern Tanzania. The differences in RMSE are more substantial in southern Africa, where the Extended WRSI has the largest wet bias (exceeding 10%), and correspondingly, has a RMSE that is more than 5 WRSI units less than the WRSI Outlook in southern Angola, central Zimbabwe, central and southern Mozambique, and southern Madagascar. **All Seasons (Figure 7d)**: Overall, the RMSE, when averaged over all years, is fairly comparable between the two methods. The increase in accuracy when using the WRSI Outlook in dry seasons (Figure 1a) is largely

33

offset by the decrease in accuracy in wet seasons (Figure 1c). The RMSE of the WRSI
Outlook is 2-5 WRSI smaller than that of the Extended WRSI in Tanzania, Malawi, southern
Namibia, southern Zambia, northern Zimbabwe, central and southern Mozambique, and
southern Madagascar. These areas indicate where the variability of the historical WRSI is the
greatest, and correspondingly, the conservative estimate provided by the WRSI Outlook has
fewer large errors than does the heavily biased Extended WRSI (the calculation of the RMSE
naturally *punishes* larger errors more so than smaller errors, and thus tends to *favor* more
conservative estimates). This is particularly evident early in the season, when the disparities
between the two forecast methods are largest.

While the accuracy results detailed here are predominantly artifacts of the systematic
biases of the Extended WRSI method, they illustrate how these biases could result in a failure
to identify drought conditions (or worse, falsely project above-average conditions).

# 4   Discussion

There are two fundamental reasons for the expected bias in the Extended WRSI,
which are described in more detail in Section 2.2A. Firstly, using average precipitation
inherently results in a roughly bell-shaped curve, with consistently wet (i.e., non-zero)
dekads. In reality, a given rainy season will have intraseasonal variability, in which wet
dekads may be interspersed with abatement or absence of rain. The greater the intraseasonal
variability in a given season (e.g., more frequent dry dekads, or longer rainy seasons), the
larger the expected impact using average inputs would have on the water satisfaction
calculation. Secondly, there exists a tendency for precipitation and evapotranspiration to be

34

inversely correlated; evapotranspiration tends to be relatively higher (lower) when precipitation is lower (higher), primarily as a result of higher (lower) solar radiation and lower (higher) relative humidity. A complementary relationship between AET and RefET provides a further nuanced relationship in the ratio of water supply and atmospheric demand, which is particularly important in characterizing drought conditions, as the elevated potential evapotranspiration exacerbates the water stress experienced in times of lower-than-average precipitation. Due to the fact that using a long-term average inherently results in a loss of these finer-time-scale relationships, the expectation was that the current practice of using climatology inputs is inadequate for accurately predicting end-of-season crop-water satisfaction. More specifically, we anticipated the Extended WRSI would overestimate water satisfaction when monitoring dry and average years, be closer to the *true* water satisfaction in wet years, and, overall, have an average predicted WRSI that was consistently larger than the true historical average (wet bias).

The removal of the systematic biases associated with the existing WRSI projection methodology is critical for the effectiveness of the WRSI as a monitoring tool for early and accurate aid allocation. The Extended WRSI method does indeed have a tendency to significantly overestimate crop-water satisfaction in large portions of all three regions (west, east, and southern Africa), as well as significantly underestimate the average crop-water satisfaction in southwestern Africa. In contrast, it is shown that the WRSI Outlook methodology of taking the mean of a series of historically based scenarios provides a relatively unbiased alternative to the Extended WRSI. As such, the WRSI Outlook is much

closer to the initial intention of the Extended WRSI: *what would the EOS WRSI of the forecasted season be if the remainder of the season resembled that of years past?*

While increased accuracy is a welcome byproduct, it should be noted once again that the primary initiative of this thesis is to provide an alternative, unbiased methodology for projecting end-of-season WRSI. Furthermore, due to the significant biases of the Extended WRSI documented in Section 3.1, and the fact that both forecasts are based solely upon the climatological statistics for a region rather than the dynamical implications of the current conditions, it should be noted that any changes in the *accuracy* of the two methodologies are more due to the change in mean value of the projections, and less due to their actual prediction capabilities. For example, the significant wet bias of the Extended WRSI naturally results in projections that resemble above-average (wet) seasons, and thus, the RMSE during those years is low. Furthermore, the Extended WRSI RMSE is doubly high during below-average (dry) seasons. In contrast, the WRSI Outlook is a conservative estimate, and therefore, it slightly overestimates dry seasons, slightly underestimates wet seasons, and is fairly *accurate* during average seasons. As mentioned previously, these traits are most noticeable early in the season, when forecast data makes up a majority of the climatological inputs of the WRSI projection. As the season progresses, and forecast data is replaced with prevailing conditions for the season in question, the two methods' projections converge on the actual EOS result.

There were several attempts to identify methods of selecting analog years (as opposed to using all historical scenarios). One such method involves to-date precipitation ranking to group historical seasons into more-likely relevant analog years. While this is an interesting

avenue for further research, the results were inconsistent, and where improved accuracy was seen, the improvements were not substantial enough (< 5 WRSI accuracy improvement) to warrant the significant increase in computations required. With that said, the results of the CHC Outlook using mean scenarios are highly encouraging, and are a marked improvement to the existing method of using climatology inputs (i.e., Extended WRSI), particularly in regards to the reduction in bias.

# 5    Concluding Remarks

Agroclimatic monitoring, and, in particular, drought early warning and forecasting, is a rapidly advancing science. Dozens of organizations, including FEWS NET, USGS/EROS, NASA, and the CHC, are working tirelessly to expand the tools available for predicting and identifying hydroclimatic conditions that contribute to food insecurity. This information helps to guide world leaders and humanitarian organizations to partition vital aid to countries around the world in a timely and precise manner.

While the WRSI is a relatively simple model, it is used widely due to its proven accuracy as a proxy for crop yield, and for its relatively little input requirements. However, the common method of using arithmetic mean climatology inputs to forecast EOS conditions (i.e., Extended WRSI) was observed to frequently produce overly optimistic outlooks. Given this, we sought to investigate the adequacy of this method for forecasting EOS WRSI. In general, the results presented here confirm a significant wet bias in the projected EOS WRSI when using arithmetic mean climatological inputs, which, among other shortcomings, significantly hinders the model's ability to capture drought events. As an alternative, we

implemented a mean scenario-based approach, which uses historical precipitation and evapotranspiration data to run out a series of historically realistic WRSI scenarios, of which the mean of these scenarios is selected as the WRSI Outlook. This method is shown to be relatively unbiased, and correspondingly, it has a considerably lower RMSE in both dry (below-average) and average seasons, relative to the commonly used method. When comparing the average accuracy of these models, the differences may seem trivial. However, the reduction in wet bias and improved accuracy during drought years is a significant step towards a more accurate and useful model. This tool is one of many in a suite of indices that are used to identify environmental stresses that may lead to increased food insecurity in rainfed agricultural areas around the world. Systematic biases, such as the wet bias seen early in the season when using the Extended WRSI, are particularly detrimental to the effectiveness of in-season monitoring, as one indicator's overly optimistic end-of-season outlook for a given area may result in that area not getting the monitoring attention it deserves later in the season, thereby shortening the delicate timeline for timely humanitarian assistance. It is our hope that this mean scenario-based approach will replace the existing arithmetic mean Extended WRSI methodology currently used by FEWS NET partners, so as to provide a more accurate approach for predicting crop water requirements, and more generally, to continue to improve the suite of tools used to identify climate and weather-related shocks to food-insecure regions.

Future research could utilize forecasts tuned to existing climate conditions to either create selection criteria for relevant analog years (as opposed to running out with all years of historical data), or, if skilled downscaled forecasts are available, replace the scenarios

entirely. In either case, this improved mean-scenario climatological forecast is essential, as it serves as an unbiased baseline to be improved upon.

# 6    References

AGRHYMET. (1996). Méthodologie de suivi des zones à risque. AGRHYMET FLASH, Bulletin de Suivi de la Campagne Agricole au Sahel. Centre Regional AGRHYMET: B.P. 11011, Niamey, Niger; 2(0/96) 1–2. Available: https://unesdoc.unesco.org/ark:/48223/pf0000121250_fre

Agutu, N.O., Awange, J.L., Zerihun, A., Ndehedehe, C.E., Kuhn, M., & Fukuda, Y. (2017). Assessing multi-satellite remote sensing, reanalysis, and land surface models' products in characterizing agricultural drought in East Africa. Remote Sensing of Environment, 194, 287–302. https://doi.org/10.1016/j.rse.2017.03.041

Archer E.R.M., Landman W.A., Tadross M.A., Malherbe J., Weepener H., Maluleke P., Marumbwa, F.M. (2017). Understanding the evolution of the 2014–2016 summer rainfall seasons in southern Africa: Key lessons. Climate Risk Management, 16: 22–28. https://doi.org/10.1016/j.crm.2017.03.006

Ayehu, G.T., Tadesse, T., Gessesse, B., & Dinku, T. (2017). Validation of new satellite rainfall products over the Upper Blue Nile Basin, Ethiopia. Atmospheric Measurement Techniques, 11(4), 1921-1936. https://doi.org/10.5194/amt-11-1921-2018

Bouchet, R. J. (1963). Evapotranspiration réelle et potentielle, signification climatique. Int. Assoc. Sci. Hydrol., Proc. Berkeley, Calif., Symp., Publ., 62 (1963), pp. 134-142. Available: https://iahs.info/uploads/dms/iahs_062_0134.pdf

Brown, M.E., Antle, J.M., Backlund, P., Carr, E.R., Easterling, W.E., Walsh, M.K., Ammann, C., Attavanich, W., Barrett, C.B., Bellemare, M.F., Dancheck, V., Funk, C., Grace, K., Ingram, J.S.I., Jiang, H., Maletta, H., Mata, T., Murray, A., Ngugi, M., Ojima, D., O'Neill, B., & Tebaldi, C. (2015). Climate Change, Global Food Security, and the U.S. Food System. 146 pages. Available online at http://www.usda.gov/oce/climate_change/FoodSecurity2015Assessment/FullAssessment.pdf.

Collischonn, B. & Collischonn, W. (2016). Rainfall as a proxy for evapotranspiration predictions. Proceedings of the International Association of Hydrological Sciences. 374. 35-40. https://doi.org/10.5194/piahs-374-35-2016

Davenport, F., Husak, G., Jayanthi, H. (2015). Simulating regional grain yield distributions to support agricultural drought risk assessment, Applied Geography, 63: 136-145. https://doi.org/10.1016/j.apgeog.2015.06.010

Dinku, T., Ceccato, P., Grover-kopec, E., Lemma, M., Connor, S.J., & Ropelewski, C.F. (2007). Validation of satellite rainfall products over East Africa's complex topography. International Journal of Remote Sensing, 28, 1503–1526. https://doi.org/10.1080/01431160600954688

Dinku, T., Funk, C., Peterson, P., Maidment, R., Tadesse, T., Gadain, H., & Ceccato, P. (2018). Validation of the CHIRPS Satellite Rainfall Estimates over Eastern of Africa. Quarterly Journal of the Royal Meteorological Society, 144, 292-312. https://doi.org/10.1002/qj.3244

DuBois, M., Harvey, P., & Tylor, G. (2018). Rapid Real-Time Review: DFID Somalia Drought Response. Department for International Development (DFID), February. Available: https://www.humanitarianoutcomes.org/publications/rapid-real-time-review-dfid-somalia-drought-response

Dunning, C. M., Black, E. C. L., & Allan R. P. (2016). The onset and cessation of seasonal rainfall over Africa. Journal of Geophysical Research: Atmospheres, 121(11), 405–11, 424. https://doi.org/10.1002/2016JD025428

FAO, 1977. Crop water requirements. FAO Irrigation and Drainage Paper No. 24, by J. Doorenbos and W.O. Pruitt. FAO, Rome, Italy. Available: http://www.fao.org/3/a-f2430e.pdf

FAO, 1979. Agrometeorological crop monitoring and forecasting. FAO Plant Production and Protection Paper No. 17, by M. Frère and G.F. Popov. FAO, Rome, Italy. Available: http://eprints.icrisat.ac.in/13138/

FAO, 1986. Yield response to water. FAO Irrigation and Drainage Paper No. 33, by J. Doorenbos, J.M.G.A. Plusje, A.H. Kassam, V. Branscheid, C.L.M. Bentvelsen. FAO, Rome, Italy.

FAO, 1998. Crop Evapotranspiration: Guidelines for Computing Crop Water Requirements. Irrigation and Drainage Paper 56, by R.G. Allen, L.S. Pereira, D. Raes, and M. Smith. FAO, Rome, Italy. Available: http://www.fao.org/3/x0490e/x0490e00.htm

FAO, 2019. Crop Prospects and Food Situation - Quarterly Global Report no. 4, December 2019. FAO, Rome, Italy. Available: http://www.fao.org/documents/card/en/c/ca7236en

FAO, IFAD, UNICEF, WFP and WHO, 2019. The State of Food Security and Nutrition in the World 2019. Safeguarding against economic slowdowns and downturns. FAO, Rome, Italy. Available: https://www.wfp.org/publications/2019-state-food-security-and-nutrition-world-sofi-safeguarding-against-economic

FAO-UNESCO, 1988. Soil map of the world: Revised legend (with corrections and updates). World Soil Resources Report 60, FAO, Rome, Italy. Available: https://www.isric.org/sites/default/files/isric_report_1988_01.pdf

FEWS NET, 2020. Global - Food Assistance Outlook Brief: Tue, 2020-03-24 | Famine Early Warning Systems Network. [cited 30 Jun 2020]. Available: https://fews.net/global/food-assistance-outlook-brief/march-2020

Funk, C., Davenport, F., Harrison, L., Magadzire, T., Galu, G., Artan, G.A., Shukla, S., Korecha, D., Indeje, M., Pomposi, C., Macharia, D., Husak, G., & Nsadisa, F.D. (2018). Anthropogenic Enhancement of Moderate-to-Strong El Niño Events Likely Contributed to Drought and Poor Harvests in Southern Africa During 2016. Bulletin of the American Meteorological Society, 99: S91–S96. https://doi.org/10.1175/BAMS-D-17-0112.1

Funk, C., Pedreros, D, Nicholson, S., Hoell, A., Korecha, D., Galu, G., Artan, G., Segele, Z., Tadege, A., Teshome, Z.A.F., Hailermariam, K., Harrison, L., Pomposi, C. (2019). Examining the Potential Contributions of Extreme "Western V" Sea Surface Temperatures to the 2017 March–June East African Drought. Bulletin of the American Meteorological Society, 100: S55–S60. https://doi.org/10.1175/BAMS-D-18-0108.1

Funk, C., Peterson, P., Landsfeld, M. Pedreros, D., Verdin, J., Shukla, S., Husak, G., Rowland, J., Harrison, L., Hoell, & A., Michaelson, J. (2015b). The climate hazards infrared precipitation with stations—a new environmental record for monitoring extremes. Sci Data 2, 150066 (2015). https://doi.org/10.1038/sdata.2015.66

Funk, C., Verdin, A., Michaelsen, J., Peterson, P., Pedreros, D., & Husak, G. (2015a). A global satellite assisted precipitation climatology. Earth Syst. Sci. Data Discuss. 7: 1-13. https://doi.org/10.5194/essd-7-275-2015

Funk, C., & Shukla, S. (2020). Drought Early Warning and Forecasting: Theory and Practice. Elsevier. https://doi.org/10.1016/C2016-0-04328-0

Funk, C., Shukla, S., Thiaw, W.M., Rowland, J., Hoell, A., McNally, A., Husak, G., Novella, N, Budde, M., Peters-Lidard, C., Adoum, A., Galu, G., Korecha, D., Magadzire, T., Rodriguez, M., Robjhon, M., Bekele, E., Arsenault, K., Peterson, P., Harrison, L., Fuhrman, S., Davenport, F., Landsfeld, M., Pedreros, D., Jacob, J.P., Reynolds, C., Becker-Reshef, I., & Verdin, J. (2019). Recognizing the Famine Early Warning Systems Network: Over 30 Years of Drought Early Warning Science Advances and Partnerships Promoting Global Food Security. Bull. Amer. Meteor. Soc., 100, 1011–1027. https://doi.org/10.1175/BAMS-D-17-0233.1

Gesch, D.B., Verdin, K.L., & Greenlee, S.K. (1999). New land surface digital elevation model covers the Earth. EOS, Transactions of the AmericanGeophysical Union, Vol. 80, No. 6, pp. 69–70. https://doi.org/10.1029/99EO00050

Hobbins, M.T., McNally, A.L., Sarmiento, D.P., Jansma, T., Husak, G.J., Turner, W., & Verdin, J.P. (2020). Using a new evaporative demand reanalysis to understand the demand perspective of drought and food insecurity in Africa. 100th American Meteorological Society Annual Meeting, Boston, MA, 12-16 January. (Oral). Available: https://ams.confex.com/ams/2020Annual/webprogram/Paper369668.html

Hobbins, M.T., McNally, A.L., Sarmiento, D.P., & Verdin, J.P. (2019b). Drought in Africa: Understanding and exploiting the demand perspective using a new evaporative demand reanalysis. European Meteorological Society Annual Meeting, Copenhagen, Denmark, 9-13 September. (Poster). Available: https://meetingorganizer.copernicus.org/EMS2019/EMS2019-791.pdf

Hobbins, M.T., Dewes, C.F., Hoell, A., Jayanthi, H., McNally, A.L., Sarmiento, D.P., Shukla, S., & Verdin, J.P. (2019a). Developing and exploiting a new global reanalysis of evaporative demand for global food-security assessments and drought monitoring. 99th American Meteorological Society Annual Meeting, Phoenix, AZ, 6-10 January. (Oral). Available: https://ams.confex.com/ams/2019Annual/meetingapp.cgi/Paper/354653

Hobbins M.T., Harrison, L.S., Blakeley, S.L., Dewes, C.F., Husak, G.J., Shukla, S., Jayanthi, H., McNally, A.L., Sarmiento, D.P., & Verdin, J.P. (2018). Drought in Africa: Understanding and exploiting the demand perspective using a new evaporative demand reanalysis. Abstract GC21D-1121, 2018 Fall Meeting, AGU, Washington, D.C., 10-14 December. (Poster). Available: https://agu.confex.com/agu/fm18/meetingapp.cgi/Paper/455750

Hobbins, M., Wood, A., Streubel, D., & Werner, K. (2012). What Drives the Variability of Evaporative Demand across the Conterminous United States? Journal of Hydrometeorology, 13, 1195-1214. https://doi.org/10.1175/JHM-D-11-0101.1

Hobbins, M.T., Wood, A., McEvoy, D.J., Huntington, J.L., Morton, C., Anderson, M., & Hain, C. (2016). The evaporative demand drought index. Part I: Linking drought evolution to variations in evaporative demand. Journal of Hydrometeorology, 17, 1745-1761. https://doi.org/10.1175/JHM-D-15-0121.1

Jayanthi, H., Husak, G.J., Funk, C., Magadzire, T., Adoum, A., & Verdin, J.P. (2014). A probabilistic approach to assess agricultural drought risk to maize in Southern Africa and millet in Western Sahel using satellite estimated rainfall. International Journal of Disaster Risk Reduction, 10 (B), 490-502. https://doi.org/10.1016/j.ijdrr.2014.04.002

Knapp, K.R., Ansari, S., Bain, C.L., Bourassa, M.A., Dickinson, M. J., Funk, C., Helms, C.N., Hennon, C.C., Holmes, C., Huffman, G.J., Kossin, J.P., Lee H.-T., Loew, A., & Magnusdottir, G. (2011). Globally gridded satellite (GriSat) observations for climate studies. Bulletin of the American Meteorological Society, 92(7): 893-907. https://doi.org/10.1175/2011BAMS3039.1

Lhomme, J.-P., & Katerji, N. (1991). A simple modelling of crop water balance for agrometeorological applications. Ecological Modelling, 57 (1-2), 11-25. https://doi.org/10.1016/0304-3800(91)90052-3

Ndayisaba, F., Guo, H., Isabwe, A., Bao, A., Nahayo, L., Khan, G., Kayiranga, A., Karamage, F., & Muhire, E.N. (2017) Inter-Annual Vegetation Changes in Response to Climate Variability in Rwanda. Journal of Environmental Protection, 8, 464-481. https://doi.org/10.4236/jep.2017.84033

Ramírez, J. A., Hobbins, M.T., & Brown, T.C. (2005). Observational evidence of the complementary relationship in regional evaporation lends strong support for Bouchet's hypothesis, Geophys. Res. Lett., 32, L15401. https://doi.org/10.1029/2005GL023549

Roser, M. and Ritchie, H, 2013. Hunger and Undernourishment. Published online at OurWorldInData.org. Retrieved from: https://ourworldindata.org/hunger-and-undernourishment [accessed 30 June 2020]

SADC: Regional Humanitarian Appeal, June 2016 - Zimbabwe. In: ReliefWeb [Internet]. [cited 30 Jun 2020]. Available: https://reliefweb.int/report/zimbabwe/sadc-regional-humanitarian-appeal-june-2016

Salerno, J., Diem, J. E., Konecky, B. L., & Hartter, J. (2019). Recent intensification of the seasonal rainfall cycle in equatorial Africa revealed by farmer perceptions, satellite-based estimates, and ground-based station measurements. Climatic Change, 153, 123-139. https://doi.org/10.1007/s10584-019-02370-4

Senay G.B., and Verdin J.P. (2002). Evaluating the performance of a crop water balance model in estimating regional crop production. Proceedings of the Pecora Symposium 15/Land Satellite Information IV/ISPRS Commission I/FIEOS 2002. Denver CO. Available: https://pdfs.semanticscholar.org/877c/5c1be1bdb6185d8f9cc54e2242e82424b73b.pdf

Senay, G.B. and Verdin, J., 2003. Characterization of yield reduction in Ethiopia using a GIS-Based crop water balance model. Canadian Journal of Remote Sensing, 29(6): 687-692. https://doi.org/10.5589/m03-039

Shukla, S., Arsenault, K.R., Hazra, A., Peters-Lidard, C., Koster, R.D., Davenport, F., Magadzire, T., Funk, C., Kumar, S., McNally, A., Getirana, A., Husak, G., Zaitchik, B., Verdin, J., Nsadisa, F.D., & Becker-Reshef, I. (2020). Improving early warning of drought-driven food insecurity in southern Africa using operational hydrological monitoring and forecasting products. Natural Hazards and Earth System Sciences, 20: 1187–1201. https://doi.org/10.5194/nhess-20-1187-2020

Thornthwaite, C. W. (1948). An approach toward a rational classification of climate. Geographical Review, 38, 55-94. https://doi.org/10.2307/210739

UNDP, 2018. Somalia Drought Impact and Needs Assessment | UNDP. [cited 30 Jun 2020]. Available: https://www.undp.org/content/undp/en/home/librarypage/climate-and-disaster-resilience-/somalia-drought-impact-and-needs-assessment.html

Verdin, J. & Klaver, R. (2002). Grid-cell-based crop water accounting for the Famine Early Warning System. Hydrological Processes, 16 (8): 1617-1630. https://doi.org/10.1002/hyp.1025

World Meteorological Organization. 1992. International Meteorological Vocabulary, 2nd edn. WMO: Geneva, Switzerland. WMO Publication 182. Available: https://library.wmo.int/doc_num.php?explnum_id=4712

WFP. (2019). The State of Food Security and Nutrition in the World (SOFI): Safeguarding against economic slowdowns and downturns | World Food Programme. [cited 30 Jun 2020]. Available:

https://www.wfp.org/publications/2019-state-food-security-and-nutrition-world-sofi-safeguarding-against-economic

WFP. (2020). 2020 Global Report on Food Crises | World Food Programme. [cited 30 Jun 2020]. Available: https://www.wfp.org/publications/2020-global-report-food-crises

Zhan, W., Guan, K., Sheffield, J., & Wood, E.F. (2016). Depiction of drought over sub‑Saharan Africa using reanalyses precipitation data sets. Journal of Geophysical Research, 121(18), 10555-10574. https://doi.org/10.1002/2016JD024858